

See discussions, stats, and author profiles for this publication at: <https://www.researchgate.net/publication/258425312>

# Metal-Chelating 2-Hydroxyphenyl Amide Pharmacophore for Inhibition of Influenza Virus Endonuclease

ARTICLE in MOLECULAR PHARMACEUTICS · NOVEMBER 2013

Impact Factor: 4.38 · DOI: 10.1021/mp400482a · Source: PubMed

---

CITATIONS

7

---

READS

65

## 9 AUTHORS, INCLUDING:



Alessia Bacchi

Università degli studi di Parma

185 PUBLICATIONS 2,627 CITATIONS

[SEE PROFILE](#)



Gabriele Rispoli

Università degli studi di Parma

18 PUBLICATIONS 158 CITATIONS

[SEE PROFILE](#)



Emilia Fisicaro

Università degli studi di Parma

109 PUBLICATIONS 1,561 CITATIONS

[SEE PROFILE](#)



Annelies Stevaert

University of Leuven

10 PUBLICATIONS 37 CITATIONS

[SEE PROFILE](#)

## Metal-Chelating 2-Hydroxyphenyl Amide Pharmacophore for Inhibition of Influenza Virus Endonuclease

Mauro Carcelli,<sup>\*,†</sup> Dominga Rogolino,<sup>†</sup> Alessia Bacchi,<sup>†</sup> Gabriele Rispoli,<sup>†</sup> Emilia Fisicaro,<sup>‡</sup> Carlotta Compari,<sup>‡</sup> Mario Sechi,<sup>§</sup> Annelies Stevaert,<sup>||</sup> and Lieve Naesens<sup>||</sup>

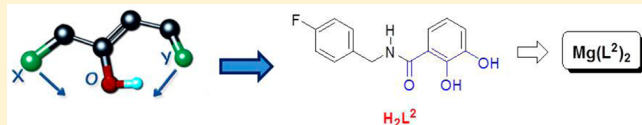
<sup>†</sup>Dipartimento di Chimica,<sup>‡</sup>Dipartimento di Farmacia, Università di Parma, Parco Area delle Scienze 17/A, 43124 Parma, Italy

<sup>§</sup>Dipartimento di Chimica e Farmacia, Università di Sassari, Via Vienna 2, 07100 Sassari, Italy

<sup>||</sup>Rega Institute for Medical Research, KU Leuven, B-3000 Leuven, Belgium

**ABSTRACT:** The influenza virus PA endonuclease is an attractive target for development of novel anti-influenza virus therapeutics. Reported PA inhibitors chelate the divalent metal ion(s) in the enzyme's catalytic site, which is located in the N-terminal part of PA (PA-Nter). In this work, a series of 2-hydroxybenzamide-based compounds have been synthesized and biologically evaluated in order to identify the essential pharmacophoric motif, which could be involved in functional sequestration of the metal ions (probably  $Mg^{2+}$ ) in the catalytic site of PA. By using  $HL^1$ ,  $H_2L^2$ , and  $HL^3$  as model ligands with  $Mg^{2+}$  ions, we isolated and fully characterized a series of complexes and tested them for inhibitory activity toward PA-Nter endonuclease.  $H_2L^2$  and the corresponding  $Mg^{2+}$  complex showed an interesting inhibition of the endonuclease activity. The crystal structures of the uncomplexed  $HL^1$  and  $H_2L^2$  and of the isolated magnesium complex  $[Mg(L^3)_2(MeOH)_2] \cdot 2MeOH$  were solved by X-ray diffraction analysis. Furthermore, the speciation models for  $HL^1$ ,  $H_2L^2$ , and  $HL^3$  with  $Mg^{2+}$  were obtained, and the formation constants of the complexes were measured. Preliminary docking calculations were conducted to investigate the interactions of the title compounds with essential amino acids in the PA-Nter active site. These findings supported the “two-metal” coordination of divalent ions by a donor triad atoms chemotype as a powerful strategy to develop more potent PA endonuclease inhibitors.

**KEYWORDS:** metalloenzymes, influenza virus endonuclease, metal chelation, antiviral, magnesium complexes



### INTRODUCTION

Seasonal human influenza A or B virus infections are an important cause of morbidity and mortality, particularly in children and elderly, chronically ill, or immunocompromised individuals. In addition, influenza A viruses are responsible for sporadic pandemics such as the 1918 “Spanish flu”<sup>1</sup> or the swine-origin A/H1N1 virus that emerged in 2009.<sup>2</sup> There is concern that highly virulent avian viruses such as A/H5N1 or the recently emerged A/H7N9 virus may cause severe pandemics when acquiring human-to-human transmissibility.<sup>3–5</sup> Influenza vaccination is the most widely used prophylactic measure, but since the development of a new pandemic vaccine requires several months, effective antiviral drugs should be available at all times. Anti-influenza virus drugs that target the viral M2 ion channel (amantadine and rimantadine) or neuraminidase (NA) (zanamivir and oseltamivir) have proven to be efficient drugs.<sup>6,7</sup> However, due to the emergence of influenza viruses showing resistance to M2 or NA inhibitors, there is an urgent need for entirely novel antiviral compounds with a different mode of action and targeting a critical step in the viral replication process.<sup>8,9</sup>

The influenza virus genome consists of eight single-stranded (-)RNA segments, which are transcribed and replicated by the viral RNA-dependent RNA polymerase (RdRp).<sup>10,11</sup> The influenza virus RdRp represents an attractive target for the development of new antiviral agents, since it is highly conserved

among influenza A, B, and C viruses, and its functions are essential for viral genome replication. The RdRp is composed of three subunits: PA, PB1, and PB2. The endonuclease activity, which resides in the N-terminal part of PA (PA-Nter), is required to cleave host cell pre-mRNAs to produce the 5'-capped primers for transcription of the viral genomic RNA into mRNA.<sup>12</sup> The protein structure of PA-Nter was described in recent crystallographic studies, which located two<sup>13</sup> or one<sup>14</sup> divalent metal ions in the active site. Recently, Crepin et al.<sup>15</sup> demonstrated that  $Mn^{2+}$  binds tightly to one site and both  $Mg^{2+}$  and  $Mn^{2+}$  can bind with lower affinity at a second site. The two-metal-ion model<sup>16</sup> is consistent with biochemical studies indicating cooperative activation by the two-metal ions.<sup>17</sup> Similar to other metal-dependent viral enzymes, that is, HIV integrase (IN) or RNase H,<sup>17</sup> metal chelation represents a relevant strategy to develop inhibitors of the PA endonuclease because compounds that efficiently coordinate the metal ions within the active site can block the enzymatic activity and prevent processing of the biological substrates (Figure 1).<sup>19,20</sup> A major breakthrough in this field was the introduction of Raltegravir, the first HIV IN inhibitor to be approved by the

Received: August 14, 2013

Revised: October 24, 2013

Accepted: November 8, 2013

Published: November 8, 2013

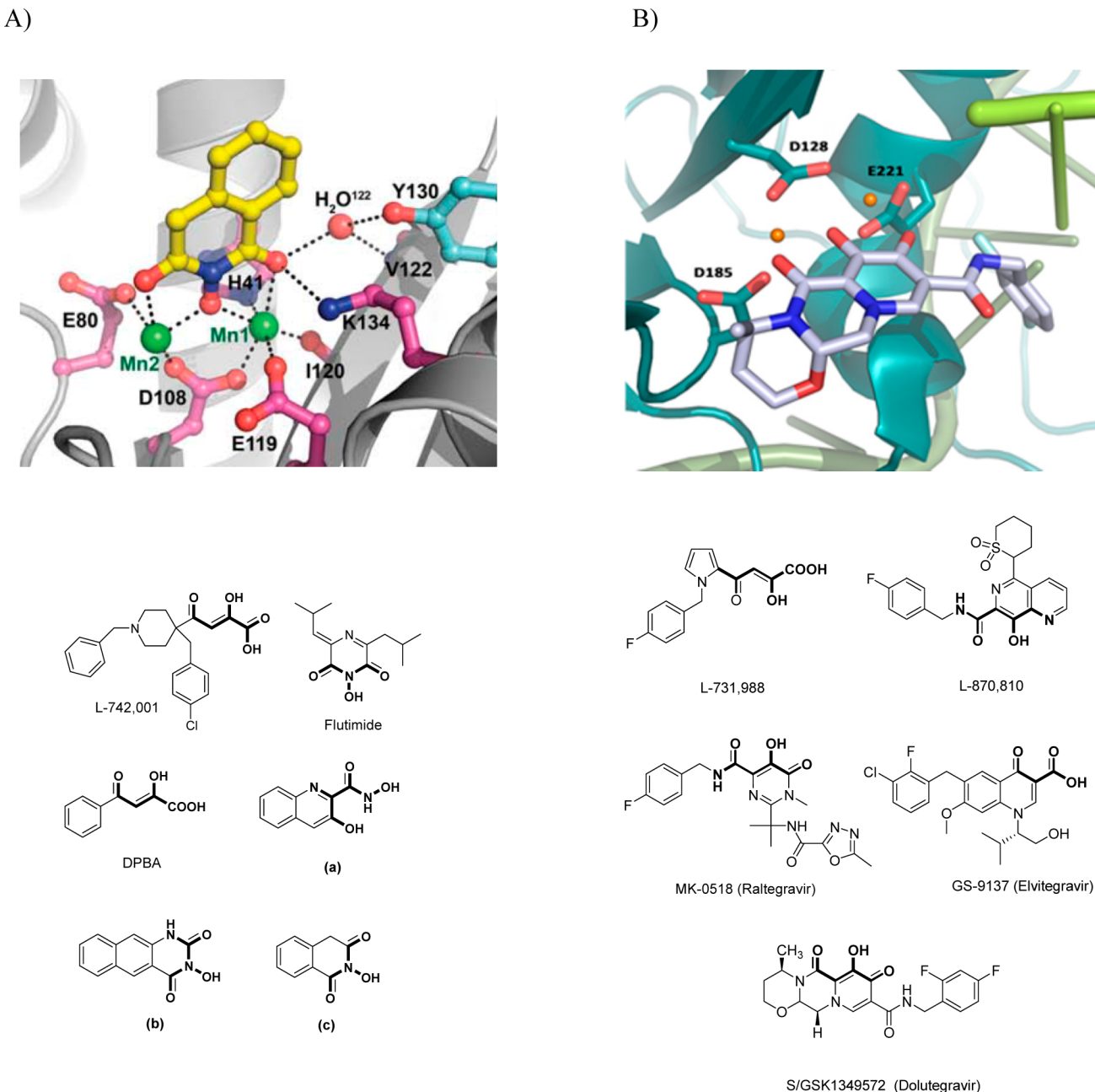


**Figure 1.** (A) (Top) Crystal structure of the active site of  $\text{PA}_N$  with the inhibitor (c) (adapted from ref 31); (bottom) some representative influenza endonuclease inhibitors with their common chelating chemotype in bold. (B) (Top) Crystal structure of the HIV-1 IN inhibitor Dolutegravir within the active site of PFV intasome [Mn(II) ions are depicted as orange spheres (adapted from Hare, S.; et al. *Mol. Pharmacol.*, **80** (2011), 565)]; (bottom) the most important metal-chelating inhibitors of HIV-1 IN with the common chelating chemotype in bold.

U.S. FDA. Similarly, diverse metal-chelating molecules have been reported to inhibit the influenza virus endonuclease activity, starting from the  $\beta$ -diketoacid family (exemplified by 2,4-dioxo-4-phenylbutanoic acid or DPBA and L-742 001, Figure 1), which are structurally related to some well-known HIV-1 IN inhibitors.<sup>21,22</sup> Metal-chelating inhibitors of the influenza virus endonuclease belonging to other chemical classes include (Figure 1): flutimide,<sup>23,24</sup> *N*-hydroxamic acids (a),<sup>25</sup> and *N*-hydroxyimides [(b) and (c)].<sup>25,26</sup> These prototype compounds share a common pharmacophoric motif that is likely responsible for functional sequestration of the metal ions in the catalytic site of PA-Nter. Other compounds such as marchantins, green tea catechins<sup>27</sup> and

dihydroxy phenethylphenylphthalimides,<sup>28,29</sup> bear a dihydroxyphenethyl group, and their action may be attributed to the dihydroxy functionality which may chelate the divalent cations within PA-Nter.<sup>28</sup> Looking at these chemotypes, it is clear that as in the case of HIV IN,<sup>30</sup> a triad of donor atoms (i.e., O, “X”, and “Y”, Figure 2) is not sufficient for potent inhibition. Rather, their optimal arrangement appears essential, along with the matching of their Lewis acid/base character. This was indeed observed in two recent studies in which the cocrystal structures of PA-Nter in complex with a variety of metal-chelating inhibitors were obtained.<sup>31,32</sup>

Recently, the salicylic acid and catechol pharmacophores were merged in a novel scaffold to create effective HIV IN

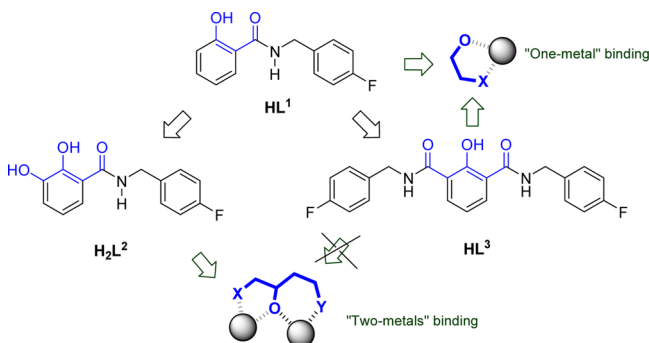


**Figure 2.** One metal (**HL<sup>1</sup>**) versus two metals binding (**H<sub>2</sub>L<sup>2</sup>** and **HL<sup>3</sup>**) 2-hydroxyphenyl amides.

inhibitors, capable of chelating two metal ions through the adjacent carboxylic and hydroxyl groups.<sup>33</sup> Due to the functional resemblance between the active sites of HIV IN and PA-Nter,<sup>18</sup> it can be hypothesized that similar molecules may be designed as effective PA endonuclease inhibitors. Accordingly, we focused our attention on three derivatives, previously tested as HIV IN inhibitors,<sup>30</sup> containing the salicylic group. In **HL<sup>1</sup>** (Figure 2), the hydroxyl and amide groups provide two essentially coplanar oxygen atoms to potentially bind one metal ion in the active site of PA-Nter. On the other hand, **H<sub>2</sub>L<sup>2</sup>** (Figure 2) contains a “two-metal” binding motif (i.e., a “O, O, O” donor atoms set) that can be involved in coordination of both ions; a similar coordinative effect can be predicted also for **HL<sup>3</sup>** (Figure 2). We herein report the synthesis and characterization of these three 2-hydroxybenzamides (**HL<sup>1</sup>, H<sub>2</sub>L<sup>2</sup>, HL<sup>3</sup>**) and the related metal complexes. We confirmed the structure of **HL<sup>1</sup>, H<sub>2</sub>L<sup>2</sup>, and [Mg-(L<sup>3</sup>)<sub>2</sub>(MeOH)<sub>2</sub>]·2MeOH** by X-ray crystallographic analysis. The metal-bonding ability of **HL<sup>1</sup>, H<sub>2</sub>L<sup>2</sup>, and HL<sup>3</sup>** toward magnesium was studied in solution and solid state. Finally, enzymatic assays were undertaken to investigate the activity of the simple ligands and of related complexes in inhibiting the endonuclease reaction performed by PA-Nter. Preliminary computational docking studies of the model ligands in the PA-Nter active site were also performed to elucidate the key features that contribute to effective metal chelation by these compounds.

## EXPERIMENTAL SECTION

**Materials and Methods. Chemistry.** All reagents of commercial quality were used without further purification. Purity of compounds was determined by elemental analysis and verified to be  $\geq 95\%$  for all synthesized molecules. NMR spectra were recorded at 25 °C on a Bruker Avance 400 FT spectrophotometer. The ATR-IR spectra were recorded by means of a Nicolet–Nexus (Thermo Fisher) spectrophotometer by using a diamond crystal plate in the range of 4000–400 cm<sup>-1</sup>. Elemental analyses were performed by using a FlashEA 1112 series CHNS/O analyzer (Thermo Fisher) with gas-chromatographic separation. Electrospray mass spectral analyses (ESI-MS) were performed with an electrospray ionization (ESI) time-of-flight Micromass 4LCZ spectrometer. MS spectra were acquired in positive EI mode by means of a DEP-probe (direct exposure probe) mounting on the tip of a Refilament with a DSQII Thermo Fisher apparatus, equipped with a single quadrupole analyzer. **HL<sup>1</sup>, H<sub>2</sub>L<sup>2</sup>, and HL<sup>3</sup>** were synthesized according to slightly modified literature procedures.<sup>30</sup>

**N-(4-Fluorobenzyl)-2-methoxybenzamide (1).** Carbonyl diimidazole (2.56 g, 15.77 mmol) was added under nitrogen to a solution of 2-methoxy benzoic acid (2 g, 13.14 mmol) in dry methylene chloride (45 mL). The solution was stirred at room temperature for 1 h. Then, 4-fluoro benzyl amine (2.25 mL, 19.71 mmol) was added, and the white suspension was stirred at room temperature for 24 h. The reaction was monitored by TLC (SiO<sub>2</sub>, eluent dichloromethane/methanol 99:1). After the complete conversion of the starting material, the reaction was quenched with 1 M HCl. The aqueous phase was extracted with methylene chloride (3 × 50 mL). The organic phases were washed with brine until neutral pH, dried on sodium sulfate, filtered, and the solvent was eliminated under reduced pressure to give the product as a light yellow oil. Yield = 97%. The product was used without further purification. <sup>1</sup>H NMR (CDCl<sub>3</sub>, 25 °C):  $\delta$  = 3.93 (s, 3H, OCH<sub>3</sub>) 4.65 (d,  $J$  = 5.7 Hz, 2H, NHCH<sub>2</sub>Ar), 6.97–7.12 (m, 4H, ArH), 7.32–7.36 (m, 2H, ArH), 7.44–7.49 (m, 1H, ArH), 8.23–8.26 (m, 2H, CONHCH<sub>2</sub>Ar, ArH). <sup>13</sup>C NMR (CDCl<sub>3</sub>, 25 °C):  $\delta$  = 165.4, 163.3, 160.8, 157.5, 134.7, 133.0, 132.4, 129.2, 121.4, 115.5, 115.3, 111.4, 56.0, 43.0. MS (EI, 70 eV)  $m/z$  (%) = 259.1 (49), 135 (100), 124.0 (31).

**N-(4-Fluorobenzyl)-2,3-dimethoxybenzamide (2).** The same as for (1), by using 2,3-dimethoxy benzoic acid (2 g, 10.98 mmol). The light beige product was used without further purification. Yield = 86%. <sup>1</sup>H NMR (CDCl<sub>3</sub>, 25 °C):  $\delta$  = 3.82 (s, 3H, OCH<sub>3</sub>), 3.90 (s, 3H, OCH<sub>3</sub>), 4.64 (d,  $J$  = 5.7 Hz, 2H, NHCH<sub>2</sub>Ar), 7.01–7.08 (m, 3H, ArH), 7.17 (t,  $J$  = 7.8 Hz, 1H, ArH), 7.32–7.37 (m, 2H, ArH), 7.73 (dd,  $J$  = 6.3 Hz,  $J$  = 1.8 Hz, 1H, ArH), 8.32 (bt, 1H, CONHCH<sub>2</sub>Ar). <sup>13</sup>C NMR (CDCl<sub>3</sub>, 25 °C):  $\delta$  = 165.2, 163.3, 160.9, 152.6, 147.5, 129.4, 129.3, 126.5, 124.5, 122.8, 115.6, 115.5, 115.4, 61.3, 56.1, 43.1. MS (EI, 70 eV)  $m/z$  (%) = 289.1 (96), 258 (30), 165.0 (100), 124.0 (53), 109.0 (40).

**N1,N3-Bis(4-fluorobenzyl)-2-methoxyisophthalamide (3).** The same as (1) by using 2-methoxy isophthalic acid (2 g, 10.2 mmol). A light pink solid was obtained after the usual workup. Yield = 90%. <sup>1</sup>H NMR (CDCl<sub>3</sub>, 25 °C):  $\delta$  = 3.65 (s, 3H, OCH<sub>3</sub>), 4.61 (d,  $J$  = 6.0 Hz, 4H, NHCH<sub>2</sub>Ar), 7.02–7.06 (m, 4H, ArH), 7.31–7.35 (m, 4H, ArH), 7.64 (bt, 2H, CONH), 8.12 (d,  $J$  = 7.6 Hz, 2H, ArH). <sup>13</sup>C NMR (CDCl<sub>3</sub>, 25 °C):  $\delta$  = 164.8, 163.4, 161.0, 155.8, 134.6, 133.9, 129.7, 127.7, 125.3, 115.8, 115.6, 63.5, 43.3. MS (EI, 70 eV)  $m/z$  (%) = 410.1 (89), 379 (7), 124 (43), 109 (100).

**N-(4-Fluorobenzyl)-2-hydroxybenzamide (HL<sup>1</sup>) (4).** To a solution of (1) (240.8 mg, 0.93 mmol) in methylene chloride (10 mL), a 1 M solution of boron tribromide in methylene chloride (5.6 mL, 5.6 mmol) at 0 °C was added, under nitrogen atmosphere. The light yellow suspension was stirred for 24 h. The reaction was monitored with TLC (SiO<sub>2</sub>; eluent dichloromethane/methanol 98:2). After the complete conversion of the starting material, the solution was diluted at 0 °C with methanol/water 2:8 (20 mL). The aqueous phase was extracted with dichloromethane (3 × 20 mL), the organic phases were washed with brine until neutral pH, dried on sodium sulfate, filtered, and the solvent was eliminated under reduced pressure to give a brown liquid. The crude product was purified by recrystallization with methanol–water to obtain the product as white solid. Yield = 77%. <sup>1</sup>H NMR (DMSO-*d*<sub>6</sub>, 25 °C):  $\delta$  = 4.50 (d,  $J$  = 5.7 Hz, 2H, CONHCH<sub>2</sub>Ar), 6.88–6.93 (m, 2H, ArH), 7.14–7.19 (m, 2H, ArH), 7.36–7.44 (m, 3H, ArH), 7.90 (dd,  $J$  = 7.5 Hz,  $J$  = 1.2 Hz, 1H, ArH), 9.36 (br,  $J$  = 5.7 Hz, 1H, CONH), 12.49 (s, 1H, OH). <sup>13</sup>C NMR (DMSO-

Table 1. Crystal Data and Structure Refinement for  $\text{HL}^1$ ,  $\text{H}_2\text{L}^2$ , and  $[\text{Mg}(\text{L}^3)_2(\text{MeOH})_2] \cdot 2\text{MeOH}$ 

	$\text{HL}^1$	$\text{H}_2\text{L}^2$	$[\text{Mg}(\text{L}^3)_2(\text{MeOH})_2] \cdot 2\text{MeOH}$
empirical formula	$\text{C}_{14}\text{H}_{12}\text{NO}_2\text{F}$	$\text{C}_{14}\text{H}_{12}\text{NO}_3\text{F}$	$\text{C}_{48}\text{H}_{50}\text{N}_4\text{O}_{10}\text{F}_4\text{Mg}$
formula weight	245.25	261.25	471.61
temperature/K	293(2)	293(2)	293(2)
crystal system	orthorhombic	orthorhombic	monoclinic
space group	$P2_12_12_1$	$Pc2_1n$	$P2_1/n$
$a/\text{\AA}$	6.494(1)	8.8140(5)	15.072(2)
$b/\text{\AA}$	11.669(2)	10.3890(5)	8.754(1)
$c/\text{\AA}$	15.492(3)	13.0280(7)	18.684(2)
$\alpha/^\circ$	90.00	90.00	90.00
$\beta/^\circ$	90.00	90.00	107.648(2)
$\gamma/^\circ$	90.00	90.00	90.00
volume/ $\text{\AA}^3$	1174.0(4)	1193.0(1)	2349.2(5)
$Z$	4	4	2
$\rho_{\text{calc}}/\text{mg/mm}^3$	1.388	1.455	1.333
$\mu/\text{mm}^{-1}$	0.104	0.113	0.116
$F(000)$	512.0	544.0	988.0
$2\Theta$ range / $^\circ$	4.38–59.42	5.58–63.88	3.06–63.88
reflections collected	17 752	18 770	37 797
independent refls [ $R(\text{int})$ ]	3321[0.0480]	3911[0.0214]	7717[0.0363]
data/restraints/parameters	3321/0/165	3911/1/181	7717/1/313
goodness-of-fit on $F^2$	0.894	0.910	1.055
final $R1$ , $wR2$ [ $I \geq 2\sigma(I)$ ]	0.0484, 0.1276	0.0334, 0.0943	0.0473, 0.1322
final $R1$ , $wR2$ [all data]	0.0723, 0.1470	0.0349, 0.0962	0.0633, 0.1445
largest $\Delta F$ max/min/e $\text{\AA}^{-3}$	0.14/–0.17	0.32/–0.19	0.53/–0.29
Flack parameter	–0.1(11)	–0.1(5)	

$d_6$ , 25 °C):  $\delta$  = 169.4, 162.9, 160.6, 135.7, 135.6, 134.3, 129.8, 129.7, 128.3, 119.1, 117.9, 115.6, 115.4, 42.2. MS (EI, 70 eV)  $m/z$  (%) = 245.0 (26), 124 (10), 121 (18), 109 (100). IR ( $\text{cm}^{-1}$ ):  $\nu_{\text{NH}}$  = 3044;  $\nu_{\text{C=O}}$  = 1632. mp 118.9–120.9 °C. Anal. Calcd for  $\text{C}_{14}\text{H}_{12}\text{FNO}_2$ : C, 68.56; H, 4.93; N, 5.71. Found: C, 68.81; H, 5.15; N, 5.59. X-ray diffraction quality crystals were obtained by recrystallization from methanol/water.

#### **N-(4-Fluorobenzyl)-2,3-dihydroxybenzamide ( $\text{H}_2\text{L}^2$ )**

(5). A 1 M solution of boron tribromide in methylene chloride (70.20 mL, 70.20 mmol) at 0 °C and in nitrogen atmosphere was added to a solution of (2) (3.3 g, 11.7 mmol) in methylene chloride (130 mL). A yellow solid was obtained after the workup already described for  $\text{HL}^1$ . The crude product was recrystallized in methanol–water. Yield = 84%.  $^1\text{H}$  NMR (DMSO- $d_6$ , 25 °C):  $\delta$  = 4.48 (d,  $J$  = 5.7 Hz, 2H, CONHCH<sub>2</sub>Ar), 6.70 (t,  $J$  = 8.1 Hz, 1H, Ar), 6.93 (d,  $J$  = 7.2 Hz, 1H, Ar), 7.14–7.20 (m, 2H, Ar), 7.32–7.40 (m, 3H, Ar), 9.19 (s, 1H, OH), 9.34 (brt,  $J$  = 5.4 Hz, 1H CONH), 12.61 (s, 1H, OH).  $^{13}\text{C}$  NMR (DMSO- $d_6$ , 25 °C):  $\delta$  = 170.2, 162.9, 150.1, 146.7, 135.6, 129.8, 129.7, 119.4, 118.5, 117.7, 115.7, 115.5, 115.4, 42.1. IR ( $\text{cm}^{-1}$ ):  $\nu_{\text{NH}}$  = 3351,  $\nu_{\text{C=O}}$  = 1644. mp 203.3–204.9 °C. Anal. Calcd for  $\text{C}_{14}\text{H}_{12}\text{FNO}_3$ : C, 64.37; H, 4.62; N, 5.35. Found: C, 63.90; H, 4.66; N, 5.34. X-ray diffraction quality crystals were obtained by recrystallization from methanol/water.

#### **N1,N3-Bis(4-fluorobenzyl)-2-hydroxyisophthalamide ( $\text{HL}^3$ ) (6).**

A 1 M solution of boron tribromide in methylene chloride was added (62 mL, 62 mmol) to a solution of (3) (4.2 g, 10.3 mmol) in methylene chloride (110 mL), at 0 °C and in nitrogen atmosphere. The light yellow suspension was stirred under nitrogen for 24 h. A gray solid was obtained after the workup already described for  $\text{HL}^1$  and  $\text{H}_2\text{L}^2$ . The crude product was recrystallized in methanol–water to obtain a white solid. Yield = 70%.  $^1\text{H}$  NMR (DMSO- $d_6$ , 25 °C):  $\delta$  = 4.53 (d,  $J$

= 5.37 Hz, 4H,  $\text{CH}_2\text{Ar}$ ), 7.03 (t,  $J$  = 7.7 Hz, 1H, Ar), 7.14–7.18 (m, 4H, Ar), 7.38–7.41 (m, 4H, Ar), 8.07 (d,  $J$  = 7.7 Hz, 2H, Ar), 9.30 (bs, 2H, CONHCH<sub>2</sub>Ar), 14.72 (s, 1H, OH).  $^{13}\text{C}$  NMR (DMSO- $d_6$ , 25 °C):  $\delta$  = 167.6, 162.9, 160.1, 135.6, 133.2, 129.8, 118.8, 115.6, 115.4, 42.4. MS (EI, 70 eV)  $m/z$  (%) = 396 (5), 124 (100), 109 (65). IR ( $\text{cm}^{-1}$ ):  $\nu_{\text{NH}}$  = 3326,  $\nu_{\text{C=O}}$  = 1645. mp 124.9–126.3 °C. Anal. Calcd for  $\text{C}_{22}\text{H}_{18}\text{F}_2\text{N}_2\text{O}_3$ : C, 66.66; H, 4.58; N, 7.07. Found: C, 66.34; H, 4.70; N, 7.03.

**Mg(L<sup>1</sup>)<sub>2</sub>·3H<sub>2</sub>O (7).** An aqueous solution of sodium hydroxide (1.02 mmol, 0.255 mL) was added to a solution of  $\text{HL}^1$  (168 mg, 0.68 mmol) in methanol (8 mL). The mixture was stirred at room temperature for 1 h. Then, a suspension of  $\text{MgCl}_2\cdot 6\text{H}_2\text{O}$  (69.12 mg, 0.34 mmol) in water (2 mL) was added. The white suspension was stirred for 24 h. The solvent was eliminated under reduced pressure to give a white solid, which was washed with water until neutral pH and then dried under vacuum. Yield = 45%.  $^1\text{H}$  NMR (DMSO- $d_6$ , 25 °C):  $\delta$  = 4.45 (bs, 2H, NHCH<sub>2</sub>Ar), 6.46 (bs, 1H, Ar), 6.66 (bs, 1H, Ar), 7.10–7.14 (m, 3H, Ar), 7.33–7.36 (m, 2H, Ar), 7.72 (bs, 1H, Ar), 10.62 (bs, 1H, NH). ESI-MS (+,  $m/z$ ): 513 [ $\text{Mg}(\text{L}^1)_2 + \text{H}^+$ ], 535 [ $\text{Mg}(\text{L}^1)_2 + \text{Na}^+$ ]. IR ( $\text{cm}^{-1}$ ):  $\nu_{\text{NH}}$  = 3380,  $\nu_{\text{CO}}$  = 1614. Anal. Calcd for  $\text{C}_{28}\text{H}_{22}\text{F}_2\text{MgN}_2\text{O}_4\cdot 3\text{H}_2\text{O}$ : C, 59.33; H, 4.98; N, 4.94. Found: C, 59.76; H, 4.84; N, 4.68.

The complexes (8) and (9) were synthesized by a similar procedure.

**Mg<sub>2</sub>(L<sup>2</sup>)<sub>2</sub>·2.5H<sub>2</sub>O (8).**  $\text{H}_2\text{L}^2$  (150 mg, 0.57 mmol) in methanol (10 mL), sodium hydroxide (1.14 mmol, 0.570 mL), and an aqueous suspension of  $\text{MgCl}_2\cdot 6\text{H}_2\text{O}$  (59 mg, 0.29 mmol) were used. The product was isolated as a white solid. Yield = 43%. IR ( $\text{cm}^{-1}$ ):  $\nu_{\text{NH}}$  = 3434,  $\nu_{\text{C=O}}$  = 1613.  $^1\text{H}$  NMR (DMSO- $d_6$ , 25 °C):  $\delta$  = 3.38 (vbs, 2H, NHCH<sub>2</sub>Ar), 6.48–7.68 (vbs, 7H, Ar), 8.59 (vbs, 1H, NH). ESI-MS (+,  $m/z$ ): 284 [ $\text{Mg}_2^{2+} + \text{H}^+$ ], 589 [ $\text{Mg}_2(\text{L}^2)_2 + \text{Na}^+$ ]. Anal. Calcd for

$C_{28}H_{20}F_2Mg_2N_2O_6 \cdot 2.5H_2O$ : C, 54.94; H, 4.12; N, 4.58. Found: C, 55.02; H, 3.67; N, 4.53.

**Mg(L<sup>3</sup>)<sub>2</sub>·3H<sub>2</sub>O (9).**  $HL^3$  (100 mg, 0.25 mmol) in methanol (8 mL), sodium hydroxide (0.38 mmol, 0.095 mL), and an aqueous suspension of  $MgCl_2 \cdot 6H_2O$  (26.43 mg, 0.13 mmol,) were used. Yield = 50%. IR ( $\text{cm}^{-1}$ ):  $\nu_{C=O} = 1633$ . <sup>1</sup>H NMR (DMSO-*d*<sub>6</sub>, 25 °C):  $\delta$  = 4.21 (bs, 4H, NHCH<sub>2</sub>Ar), 6.22–8.04 (bs, 11H, Ar), 9.25 (bs, 1H, NH), 11.47 (bs, 1H, NH), 12.16 (bs, 2H, NH). ESI-MS (+, *m/z*): 419 [ $HL^3 + Na]^+$ , 837 [ $Mg(L^3)_2 + Na]^+$ . Anal. Calcd for  $C_{44}H_{34}F_4MgN_4O_6 \cdot 3H_2O$ : C, 60.81; H, 4.64; N, 6.45. Found: C, 60.70; H, 4.30; N, 6.38. X-ray diffraction quality crystals were obtained by recrystallization from methanol as  $[Mg(L^3)_2(MeOH)_2] \cdot 2MeOH$ .

**X-ray Crystallography.** Crystals suitable for X-ray diffraction were obtained by slow evaporation of methanol/water ( $HL^1$  and  $H_2L^2$ ) and methanol ( $[Mg(L^3)_2(MeOH)_2] \cdot 2MeOH$ ) solutions, respectively. X-ray diffraction data were collected at room temperature on a Bruker APEX II diffractometer equipped with CCD detector, using graphite monochromated Mo K $\alpha$  ( $\lambda = 0.71069 \text{ \AA}$ ) radiation. Resulting crystal decay was negligible. Data were processed by Lorentz and polarization corrections with the SAINT package,<sup>34</sup> corrected for absorption effects by the SADABS<sup>35</sup> procedure. The phase problem was solved by direct methods<sup>36</sup> and refined by full matrix least-squares on all  $F^2$ .<sup>37</sup> Anisotropic displacement parameters were refined for all non hydrogen atoms, while hydrogen atoms were introduced in idealized positions; only the hydrogen atoms of the OH groups of the methanol molecules in  $[Mg(L^3)_2(MeOH)_2] \cdot 2MeOH$  were located on the difference map and refined independently. The final maps were featureless. Details of data collection and structure refinement are presented in Table 1. For the discussion, use was made of the Cambridge Structural Database software<sup>38</sup> and of Olex2.<sup>39</sup> CCDC-942580-942582 contains the supplementary crystallographic data for this paper. These data can be obtained free of charge via [www.ccdc.cam.ac.uk/conts/retrieving.html](http://www.ccdc.cam.ac.uk/conts/retrieving.html) (or from the Cambridge Crystallographic Data Centre, 12 Union Road, Cambridge CB2 1EZ, UK; fax: (44) 1223-336-033; or e-mail: deposit@ccdc.cam.ac.uk).

**Potentiometry.** The Mg(II) stock solutions were prepared from  $MgCl_2 \cdot 6H_2O$  (Aldrich). Their concentrations were determined using EDTA as a titrant and the sodium salt of Eriochrome black T in the presence of triethanolamine and hydroxylamine chloride as an indicator. Equilibrium constants for protonation and complexation reactions were determined by means of potentiometric measurements in methanol/water = 9:1 v/v solution at ionic strength 0.1 M KCl, carried out at 25 ± 0.1 °C under nitrogen in the pH range 2.5–11. Temperature was controlled to ±0.1 °C by using a thermostatted circulating water bath (ISCO GTR 2000 IIx). Appropriate aliquots of ligand solution, prepared by weight, were titrated with standard KOH (methanol/water = 9:1 v/v, *I* = 0.1 M KCl) with and without metal ions, applying constant speed magnetic stirring. Freshly boiled methanol and double-distilled water, kept under nitrogen, were used throughout. The experimental procedure to reach high accuracy in the determination of the equilibrium constants in this mixed solvent has been described in detail elsewhere.<sup>40</sup> The protonation constants of  $HL^1$ ,  $H_2L^2$ , and  $HL^3$  were obtained by titrating 20–50 mL of samples of each ligand ( $3 \times 10^{-3}$  to  $5 \times 10^{-3}$  M). For the complex formation constants, the titrations were performed with different ligand/metal ratios (1 up to 5). At least two measurements (about 60 experimental points each) were performed for each system.

Potentiometric titrations were carried out by a fully automated apparatus equipped with a CRISON GLP 21–22 digital voltmeter (resolution, 0.1 mV) and a 5 mL Metrohm Dosimat 655 autoburet, both controlled by a homemade software in BASIC, working on an IBM computer. The electrode chain (Crison 5250 glass electrode and 0.1 M KCl in methanol/water = 9:1 v/v calomel electrode, Radiometer 401) was calibrated in terms of  $[H^+]$  by means of a strong acid–strong base titration by Gran's method,<sup>41</sup> allowing the determination of the standard potential,  $E^\circ$  ( $371.5 \pm 0.4$  mV), and of the ionic product of water,  $K_w$  ( $pK_w = 14.40 \pm 0.05$ ) in the experimental conditions used. The software HYPERQUAD<sup>42</sup> was used to evaluate the protonation and complexation constants from emf data.

### Biology. Production of Recombinant Influenza Virus PA-Nter Protein.

The coding sequence for PA-Nter (i.e., residues 1–217 from the PA protein of influenza virus strain A/X-31) was cloned in the pET28a(+) plasmid (Merck KGaA), and the protein was expressed in *E. coli* BL21-CodonPlus cells (Agilent Technologies) and purified by 6xHis-Ni-NTA chromatography,<sup>27</sup> followed by buffer exchange.

**Enzymatic Assay with Influenza PA-Nter Endonuclease.** The enzymatic assay was performed according to a published procedure,<sup>13</sup> with some modifications. The reaction mixture (25  $\mu\text{L}$  volume) contained 1  $\mu\text{g}$  of recombinant PA-Nter, 1  $\mu\text{g}$  (16.7 nM) of single-stranded circular DNA plasmid M13mp18 (Affymetrix), buffer (50 mM Tris-HCl pH 8, 100 mM NaCl, 1 mM MnCl<sub>2</sub>, and 10 mM  $\beta$ -mercaptoethanol), and serial dilutions of the test compounds. 2,4-Dioxo-4-phenylbutanoic acid (DPBA, purchased from Interchim), a diketo acid compound known to inhibit the influenza virus endonuclease,<sup>21</sup> was included as reference compound. After a 1 h incubation at 37 °C, the reaction was stopped by heat inactivation (80 °C, 20 min). The endonucleolytic digestion of the plasmid was visualized by gel electrophoresis on a 1% agarose gel with ethidium bromide staining. The amount of remaining intact plasmid was quantified by ImageQuant TL software (GE Healthcare).

For each active compound, the percentage inhibition of PA endonuclease activity was plotted against the compound concentration on a semilogarithmic plot, using GraphPad Prism software. Values were the mean ± SEM of three independent experiments. The 50% inhibitory concentrations ( $IC_{50}$ ) were obtained by nonlinear least-squares regression analysis.

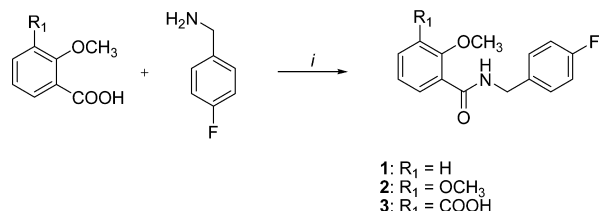
**Computational Methods.** Ligand docking studies were performed using the Molecular Operating Environment (MOE) software suite.<sup>43</sup> For docking experiments, the crystal structure of avian influenza virus PAN bound to L-742 001 was retrieved from the PDB Data Bank (<http://www.rcsb.org/> - PDB code: 4E5H).<sup>31</sup> To reduce significant differences between the A/X-31 and the HSN1 sequence of the X-ray crystal model, the residue Ala20, located quite near the active site metals, has been replaced with a threonine (A20T), which was submitted to a minimization procedure using AMBER99 force field with a generalized Born solvation model. Moreover, minimization of Arg84 has been performed to balance the shift of such residue due to the presence of L-742 001 in the cocrystal structure. Water molecules have been removed, and the partial charges were automatically calculated. The structures of compounds  $HL^1$ ,  $H_2L^2$ , and  $HL^3$  were built in MOE and minimized before the docking, using the MMFF94x force field, with the systematic algorithms until a RMSD gradient of 0.001 kcal mol<sup>-1</sup> Å<sup>-1</sup> was reached. Rigid receptor–flexible ligand (bearing

constrained chelating groups) docking calculations were performed using the docking simulation feature MOE-dock by setting grid sizes that included the entire macromolecule. The triangle matcher was used as a placement method to generate docking poses.<sup>44</sup> Only the best-scored poses generated in the docking experiments were retained and examined with MOE.

## ■ RESULTS AND DISCUSSION

**Synthesis and Characterization of  $\text{HL}^1$ ,  $\text{H}_2\text{L}^2$ ,  $\text{HL}^3$  and of the Corresponding Magnesium Complexes (7), (8), and (9).** The amides (1)–(3) were obtained with good yields (Scheme 1) and characterized by the usual spectroscopic tools.

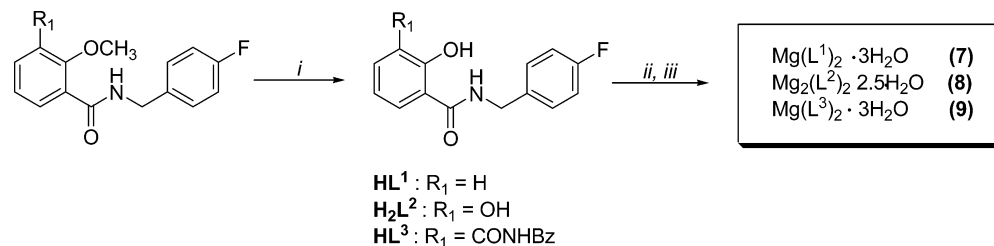
**Scheme 1. Synthesis of Amide Intermediates<sup>a</sup>**



<sup>a</sup>Reagents and conditions: (i) carbonyldiimidazole, dichloromethane dry, r.t. 24 h.

Deprotection of the hydroxyl groups (Scheme 2) was carried out with a 1 M solution of boron tribromide to obtain  $\text{HL}^1$ ,  $\text{H}_2\text{L}^2$ , and  $\text{HL}^3$ . The complexes  $\text{Mg}(\text{L}^1)_2 \cdot 3\text{H}_2\text{O}$  (7),  $\text{Mg}_2(\text{L}^2)_2 \cdot 2.5\text{H}_2\text{O}$  (8), and  $\text{Mg}(\text{L}^3)_2 \cdot 3\text{H}_2\text{O}$  (9) were synthesized by reacting in methanol the deprotonated ligands with magnesium chloride in a 2:1 ligand-to-metal ratio (Scheme 2). The use of a base is necessary to ensure deprotonation of the hydroxyl moiety and subsequent coordination to the metal. In the IR spectra of all the complexes, the OH absorption disappeared ( $2800$ – $3000$   $\text{cm}^{-1}$  in the free ligands), and the  $\text{C}=\text{O}$  bands shifted from  $1632$  to  $1644$   $\text{cm}^{-1}$  in  $\text{HL}^1$ ,  $\text{H}_2\text{L}^2$ , and  $\text{HL}^3$  to  $1613$ – $1614$   $\text{cm}^{-1}$  in the complexes because of the involvement of the amide group in coordination. In the  $^1\text{H}$  NMR spectra of the magnesium complexes, a broadening and a downfield shift of the signals of about  $0.2$  ppm was observed versus the free ligands, and the resonance of the OH proton, detectable in the free ligand, disappeared. In particular, in complex (8), both the hydroxyl groups are deprotonated, and all data are in agreement with a 2:2 metal to ligand ratio. In the  $^1\text{H}$  NMR spectrum of (9), it is also possible to distinguish the signals of the two different arms of the ligand, the coordinated and the uncoordinated one. Elemental analysis and mass spectra confirm the proposed stoichiometry.

**Scheme 2. Synthesis of the Ligands and the Corresponding Magnesium Complexes<sup>a</sup>**



<sup>a</sup>Reagents and conditions: (i)  $\text{BBr}_3$ , dichloromethane dry,  $T = 0$   $^\circ\text{C}$  to r.t., 24 h; (ii)  $\text{NaOH}$  2 M r.t. 30 min, methanol; (iii)  $\text{MgCl}_2$  r.t. 5 h.

**Discussion of the X-ray Structures of  $\text{HL}^1$ ,  $\text{H}_2\text{L}^2$ , and  $[\text{Mg}(\text{L}^3)_2(\text{MeOH})_2] \cdot 2\text{MeOH}$ .** The molecular structures of  $\text{HL}^1$  and  $\text{H}_2\text{L}^2$  are remarkably similar, with a root-mean-square deviation less than  $0.16$   $\text{\AA}$  for the superimposition of the atoms common to the two molecules (Figure 3). In fact, the main conformational degrees of freedom for both ligands are the torsion around the bonds  $\text{C}1-\text{C}7$ ,  $\text{N}1-\text{C}8$ ,  $\text{C}8-\text{C}9$ , with values of  $\text{C}2-\text{C}1-\text{C}7-\text{N}1 = 175.5(1)$ ,  $165.8(2)^\circ$ ;  $\text{C}7-\text{N}1-\text{C}8-\text{C}9 = -94.0(1)$ ,  $-96.0(2)^\circ$ ;  $\text{N}1-\text{C}8-\text{C}9-\text{C}14 = 73.4(1)$ ,  $79.8(2)^\circ$ , respectively, for  $\text{H}_2\text{L}^2$  and  $\text{HL}^1$ . In both cases, the torsion angle around the bond  $\text{C}1-\text{C}7$  is locked to a planar conformation by the intramolecular hydrogen bond between the amide carbonyl and the *o*-OH group on the adjacent aromatic ring ( $\text{O}1\cdots\text{O}2 = 2.491(1)$  and  $2.523(2)$   $\text{\AA}$ ,  $\text{O}-\text{H}\cdots\text{O} = 158(2)$  and  $147.9(1)^\circ$ , respectively, for  $\text{H}_2\text{L}^2$  and  $\text{HL}^1$ ). Combined with the constrained planarity of the amide group, this results in the overall planarity of the ligand from  $\text{C}4$  to  $\text{C}8$ . By contrast, the *p*-F-phenyl group is in both cases perpendicular to the rest of the molecule, resulting in a remarkably bent conformation (Figure 4). The crystal packing of  $\text{HL}^1$  (Figure 4) is simply based on the complete balance of hydrogen bond donors and acceptors present in the molecule, since besides the intramolecular hydrogen bond, the remaining NH donor links to the OH acceptor in chains where molecules are translated along the *a* axis ( $\text{N}1-\text{H}\cdots\text{O}1(i) = 2.992(3)$   $\text{\AA}$ ,  $143.4(1)^\circ$ ,  $i = x + 1, y, z$ ). In analogy to  $\text{HL}^1$ , in  $\text{H}_2\text{L}^2$  the NH group acts as donor toward the OH already involved in the intramolecular hydrogen bond ( $\text{N}1-\text{H}\cdots\text{O}1(ii) = 2.885(1)$   $\text{\AA}$ ,  $140(2)^\circ$ ,  $ii = 3/2 - x, y, z - 1/2$ ), thus forming screw chains where consecutive molecules are rotated by  $180^\circ$ ; the same screw motif is found in the structure of the *N*-benzyl-2-hydroxybenzamide.<sup>45</sup> The second OH group links to the amide carbonyl ( $\text{O}3-\text{H}\cdots\text{O}2(iii) = 2.675(1)$   $\text{\AA}$ ,  $169.5(1)^\circ$ ,  $iii = x + 1/2, y + 1/2, 3/2 - z$ ), originating a three-dimensional network (Figure 4) with all fluorines segregated in square channels.

The molecular structure of  $[\text{Mg}(\text{L}^3)_2(\text{MeOH})_2] \cdot 2\text{MeOH}$ , displayed in Figure 5, is a neutral centrosymmetric octahedral complex, with two deprotonated ligands on the equatorial plane and two coordinated methanol molecules at the apices (Table 2). Two methanol molecules cocrystallize in the complex, enriching the packing network. Coordination occurs by chelation of the deprotonated OH and one of the two amide carbonyl oxygens on each ligand, while the second amide  $\text{C}=\text{O}$  is free and points away from the metal in order to allow the formation of an intramolecular hydrogen bond between the NH and the central coordinated oxygen ( $\text{N}2-\text{H}\cdots\text{O}2 = 2.591(1)$   $\text{\AA}$ ,  $136.9(1)^\circ$ ). The two ligand arms show therefore opposite configuration with respect to the  $\text{C}9-\text{C}8$  and  $\text{C}13-\text{C}15$  equivalent bonds ( $\text{C}10-\text{C}9-\text{C}8-\text{N}1 = -171.6(1)^\circ$  for the coordinated amide oxygen, and  $\text{C}12-\text{C}13-\text{C}15-\text{O}3 =$

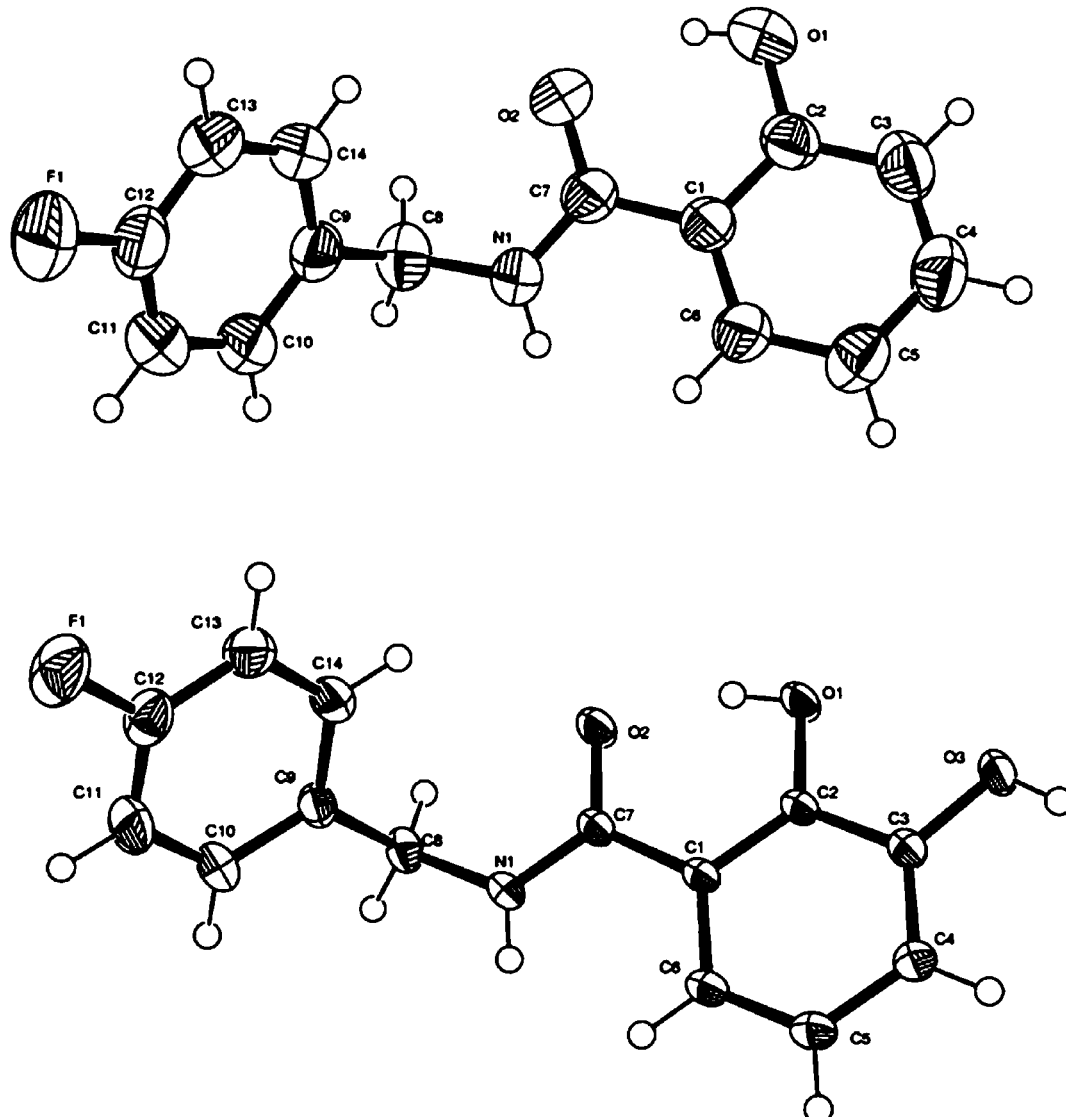


**Figure 3.** Molecular structures and labeling of  $\text{HL}^1$  (top) and  $\text{H}_2\text{L}^2$  (bottom), with thermal ellipsoids drawn at the 50% probability level.

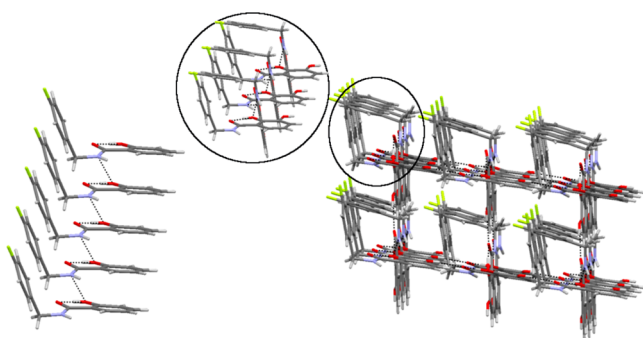


**Figure 4.** Hydrogen bond network in  $\text{HL}^1$  (left) and  $\text{H}_2\text{L}^2$  (right). The round inset highlights the screw chain motif in  $\text{H}_2\text{L}^2$ .

8.2(2) $^\circ$  for the free amide). The six-membered chelation rings are practically planar, with a slight out of plane deformation at O1. The intramolecular NH...O hydrogen bond, together with the chelation and the intrinsic planarity of the amide moieties, renders the central core of the complex quite planar (maximum deviation for the skeleton from C7 to C16 = 0.27 Å for O1). The four *p*-F-phenyl rings point away from this mean plane,

with different orientations relatively to the NH vectors: H1–N1–C7–C4 = -12.9(2) $^\circ$  for the chelating ligand arm, and H2–N2–C16–C17 = -92.4(1) $^\circ$  for the free arm.

**Potentiometric Measurements and Calculations.** The metal-binding behavior of some hydroxybenzamides has been previously investigated by computational docking studies to elucidate their interactions with the active site of the prototype foamy virus IN,<sup>30</sup> but nothing is known about the speciation of this class of ligand with magnesium. This information is essential in order to rationalize their inhibitory ability and mechanism of action. In this perspective, we carried out potentiometric studies about the solution behavior of  $\text{HL}^1$ ,  $\text{H}_2\text{L}^2$ , and  $\text{HL}^3$  with Mg<sup>2+</sup>. To be consistent with our previous studies,<sup>46</sup> the titrations have been performed in mixed solvent methanol/water = 9/1 and ionic strength 0.1 M KCl.

The acidity ( $\text{pK}_a$ ) of the salicylic OH of the ligands resulted 9.51(0.01) for  $\text{HL}^1$ , 9.10(0.01) for  $\text{H}_2\text{L}^2$ , and 7.28(0.01) for  $\text{HL}^3$ , in which the presence of two identical amido moieties in *ortho*-position to the acidic OH allows for a greater delocalization of the charge of the anion. The second acidity constant ( $\text{pK}_{a2}$ ) for  $\text{H}_2\text{L}^2$  cannot be correctly evaluated by potentiometry because it is greater than 12 and so out of the

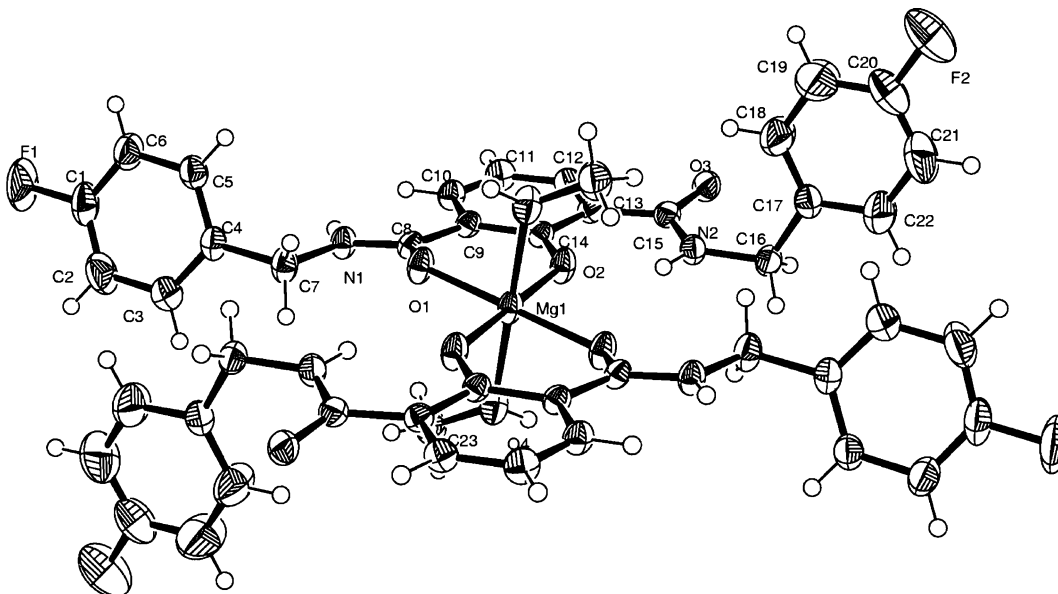


**Figure 5.** Molecular structure of the neutral complex  $[\text{Mg}(\text{L}^3)_2(\text{MeOH})_2] \cdot 2\text{MeOH}$ , with thermal ellipsoids drawn at the 50% probability level. The two cocrystallized methanol molecules are omitted.

**Table 2. Coordination Bond Lengths (Å) and Angles (°) of Magnesium in  $[\text{Mg}(\text{L}^3)_2(\text{MeOH})_2] \cdot 2\text{MeOH}$  with SD in Parentheses**

MgO1	1.9997(8)
MgO1 <sup>1</sup>	1.9997(8)
MgO2	1.9813(8)
MgO2 <sup>1</sup>	1.9813(8)
MgO4 <sup>1</sup>	2.153(1)
MgO4	2.153(1)
O1 <sup>1</sup> MgO1	180.00
O1MgO4	89.91(4)
O1MgO4 <sup>1</sup>	90.09(4)
O1 <sup>1</sup> MgO4 <sup>1</sup>	89.91(4)
O1 <sup>1</sup> MgO4	90.09(4)
O2 <sup>1</sup> MgO1 <sup>1</sup>	86.57(3)
O2MgO1 <sup>1</sup>	93.43(3)
O2 <sup>1</sup> MgO1	93.43(3)
O2MgO1	86.57(3)
O2MgO2 <sup>1</sup>	180.00
O2 <sup>1</sup> MgO4 <sup>1</sup>	90.22(4)
O2MgO4	90.22(4)
O2 <sup>1</sup> MgO4	89.78(4)
O2MgO4 <sup>1</sup>	89.78(4)
O4MgO4 <sup>1</sup>	180.00

<sup>1</sup>Symmetry operator:  $1 - x, 1 - y, -z$

limits of reliability of the glass electrode. The best fit of the experimental titration curves, carried out in presence of the metal ion, was obtained by the sets of species shown in Table 3. The proposed models are corroborated by very good statistical parameters and by nice overlapping between experimental and computed titration curves. In order to understand the speciation in solution, it must be recalled that the wide prevalence of magnesium as the metal cofactor for enzymes is due not only to its high natural abundance but also to its peculiar chemical–physical properties.<sup>47–49</sup> The  $\text{Mg}^{2+}$  ion is characterized by a small ionic radius, high charge density, and tendency to bind water molecules in the inner coordination

**Table 3. Logarithms of Formation Constants ( $\beta_{pqr} = [\text{M}_p\text{L}_q\text{H}_r]/[\text{M}]^p[\text{L}]^q[\text{H}]^r$ ) in Methanol/Water = 9:1 v/v,  $I = 0.1 \text{ M KCl}$  at  $25^\circ\text{C}$  for the ligands under study with  $\text{Mg}^{2+}$ . SDs are given in parentheses. Charges are omitted for simplicity**

$\text{HL}^1$			
$p$	$q$	$r$	$\text{Mg}^{2+}$
1	1	-1	-7.98 (0.06)
1	2	-2	-16.75 (0.48)
$\text{L} + \text{H} = \text{LH}$			
9.51 (0.01)			
$\text{H}_2\text{L}^2$			
$p$	$q$	$r$	$\text{Mg}^{2+}$
1	1	1	2.71 (0.08)
1	1	0	-5.53 (0.06)
$\text{LH} + \text{H} = \text{LH}_2$			
9.10 (0.01)			
$\text{HL}^3$			
$p$	$q$	$r$	$\text{Mg}^{2+}$
1	0	-1	-9.84 (0.07)
1	1	0	2.66 (0.16)
1	2	0	5.85 (0.09)
$\text{L} + \text{H} = \text{LH}$			
7.28 (0.01)			

sphere, rather than bulkier ligands. This also explains why many magnesium salts are extensively hydrated in the crystalline form, with the anion located in the outer coordination sphere. Crystallographic data showed that outer sphere coordination by hexahydrate magnesium is the normal binding mode of  $\text{Mg}^{2+}$  to oligonucleotides.<sup>47,48</sup> Moreover, being a “hard” ion, it prefers binding to “hard” oxygen-containing ligands, such as carbonyls, carboxylates, phosphates, hydroxyls, and water.

Despite the similar  $\text{pK}_a$  values of the salicylic OH,  $\text{HL}^1$  and  $\text{H}_2\text{L}^2$  behave very differently in solution with  $\text{Mg}^{2+}$  ions (see Table 3). For  $\text{HL}^1$ , the species  $[\text{MgLH}_-]$  and  $[\text{MgL}_2\text{H}_2]^{2-}$  were found. The species distribution plot for  $\text{HL}^1$  in Figure 6a clearly shows that the metal is not bound at physiological pH; rather, these complexes are formed in basic solution above pH 9 at which one or two water molecules of the inner

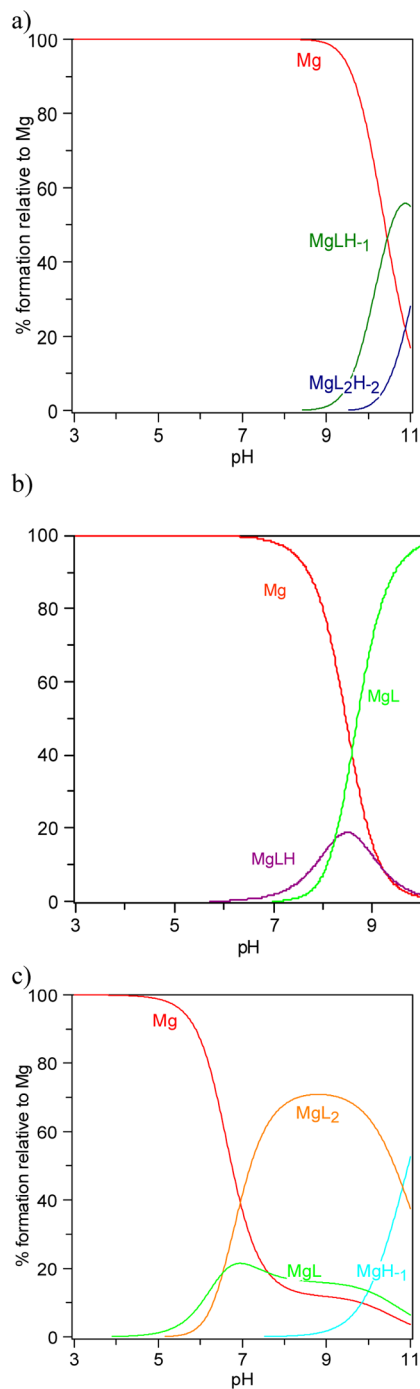


**Figure 6.** Distribution diagrams for the systems under investigation at  $\text{L:Mg} = 4:1$  (the concentration of  $\text{Mg}^{2+}$  is 25 mM): (a)  $\text{L} = \text{HL}^1$ , (b)  $\text{L} = \text{H}_2\text{L}^2$ , (c)  $\text{L} = \text{HL}^3$ .

coordination sphere loose a proton, justifying the negative index of H in the above formulas. Moreover, the complexes are formed when the ligand is in the deprotonated form, which means that the acidity of the ligand is not affected by the presence of  $\text{Mg}^{2+}$  ion, indicating an outer sphere coordination.

For  $\text{H}_2\text{L}^2$ , the species  $[\text{MgHL}]^{+1}$  and  $[\text{MgL}]$  give rise to the best fit of the experimental data. Figure 6b outlines the difference in respect to  $\text{HL}^1$ . In fact, the formation of the complexes starts at pH below 7, showing that metal ion coordination lowers the  $\text{pK}_a$  value of the salicylic OH. This strong effect suggests an inner sphere coordination. Moreover,

Figure 6b shows that the  $[\text{MgHL}]^{+1}$  complex changes into  $[\text{MgL}]$ , due to the acid dissociation of the second OH of the ligand, so forming an inner sphere chelate in a very cooperative manner. The presence on the ligand of three oxygens, over which the charges derived by the dissociation of the two OH groups are delocalized, is the condition favoring the formation of an inner sphere complex.

The situation is different for  $\text{HL}^3$ , which bears only one acidic OH between two amidic groups. It is important to underline that its coordination ability toward magnesium ions seems to be lower than that of  $\text{H}_2\text{L}^2$ . The best fit is obtained by a model considering the species  $[\text{MgL}]^{-1}$ ,  $[\text{MgL}_2]$ , and  $[\text{MgH-1}]^{-1}$ . The last one is a hydroxide species, necessary in order to achieve convergence of the fit and obtain good statistical parameters. The distribution diagram of Figure 6c shows that the complex formation starts at a pH about 5, indicating that the interaction with  $\text{Mg}^{2+}$  lowers the  $\text{pK}_a$  value of the ligand, but, notwithstanding the quite high ligand/metal ratio, the metal is never completely complexed by  $\text{HL}^3$  and its concentration decreases when the hydroxide species starts forming. This behavior does not allow the discrimination between an inner or outer sphere complex, but, considering that  $\text{HL}^3$  is a bulky ligand, the last hypothesis appears more likely.

**Inhibition of PA-Nter Endonuclease Activity.** The hydroxybenzamide-based ligands and their complexes were tested for their ability to inhibit the endonuclease activity of PA-Nter in an enzymatic assay with recombinant PA-Nter. Two compounds,  $\text{H}_2\text{L}^2$  and the corresponding magnesium complex (8), showed a dose-dependent inhibition of the endonuclease activity (Figure 7), thus demonstrating the effectiveness of this novel 2,3-dihydroxybenzamide scaffold. Interestingly, complex (8) proved to be the most active compound, with an  $\text{IC}_{50}$  value of 18  $\mu\text{M}$ , which is 6-fold higher than that of the reference compound DPBA. The uncomplexed ligand  $\text{H}_2\text{L}^2$  ( $\text{IC}_{50} = 33 \mu\text{M}$ ) had an 11-fold lower potency than DPBA. The  $\text{IC}_{50}$  value that we obtained for DPBA (3  $\mu\text{M}$ ) is comparable to that published by others,<sup>50</sup> supporting the relevance of our enzyme inhibition data. The other four compounds ( $\text{HL}^1$ ,  $\text{HL}^3$ , and the complexes (7) and (9)) did not inhibit the endonuclease reaction at 500  $\mu\text{M}$ , the highest concentration tested.

It is worth noting that the complex (8) displayed a 2-fold higher potency than its free ligand  $\text{H}_2\text{L}^2$ . This suggests that the effective inhibitor of the activity of the enzyme could be a metal complex and not a free ligand. In fact, the activity of  $\text{H}_2\text{L}^2$  could be due to the formation of the corresponding complex, when it is added to the enzymatic assay in the presence of divalent metal ions.

**Molecular Modeling.** To understand the binding mode of  $\text{HL}^1$ ,  $\text{H}_2\text{L}^2$ , and  $\text{HL}^3$  to PA-Nter protein, and to propose a plausible mechanistic hypothesis, preliminary ligand–receptor docking studies were conducted. The coordinates for PA-Nter protein (PDB code: 4E5H) were used for computational docking. On the basis of the structure and the  $\text{pK}_a$  values of the model ligands (see potentiometry section), we built compounds  $\text{HL}^1$ ,  $\text{H}_2\text{L}^2$ , and  $\text{HL}^3$  in monodeprotonated form. Graphical representations of top-ranking binding modes obtained for these ligands are depicted in Figure 8. Analysis of the docking results showed different binding modes with variable affinities within the amino acid pocket located near the catalytic site that includes the following residues: Thr20, Glu23, Tyr24, Glu26, Lys34, Ile38, His41, Glu80, Gly81, Arg82, Asp83, Arg84, Thp88, Lys104, Phe105, Leu106, Asp108,

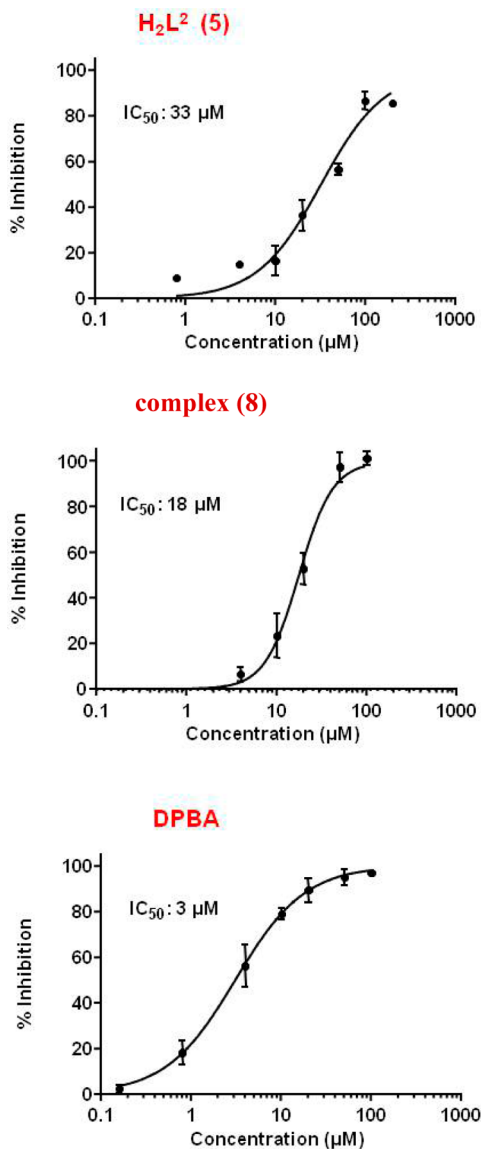


**Figure 7.** Dose-response curves for inhibition of influenza PA-Nter endonuclease activity by the two active compounds,  $\text{H}_2\text{L}^2$  and its magnesium complex 8. DPBA was included as the reference compound<sup>21</sup>. Values represent the percentage inhibition (versus the no compound control) and are the mean  $\pm$  SEM of three independent tests.

Phe117, Glu119, Ile120, Gly121, Val122, Tyr130, Lys134, Lys137, and Ile138 (Figure 8, A–C). The residues His41, Asp108, Glu119, and Lys134 are involved in metal binding and play a role in the catalytic process. In particular, the most favorable conformation places  $\text{HL}^1$  in proximity to His41, located near the metal ions (Figure 8A). The inactivity of  $\text{HL}^1$  in the enzymatic assay may be explained by the observation that this compound does not tightly interact with the metal ion and that the flexibility and the orientation of the *p*-fluorobenzyl moiety away from the pocket could reduce the formation of favorable interactions (such as  $\pi$ -stacking) with the hydrophobic residues.

On the other hand, in all docking clusters,  $\text{H}_2\text{L}^2$  was found to bind to one metal ion cofactor through the catechol group, and it also establishes a coordination bond with the second cation by a combination of the  $\alpha$ -hydroxyl and the amide-linked carbonyl groups (Figure 8B). Moreover, for the binding pose

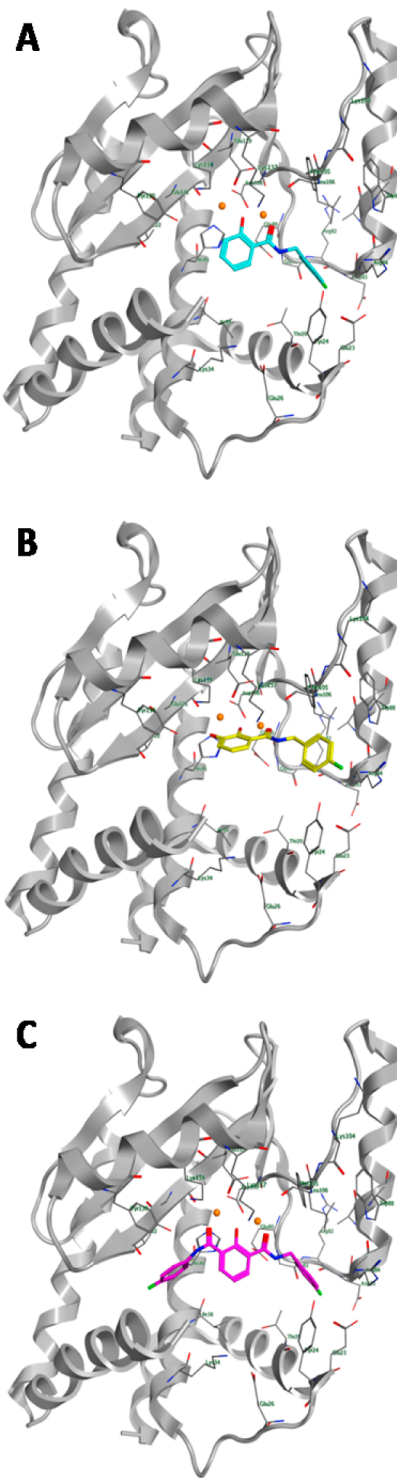


**Figure 8.** Representative view of in silico docking of  $\text{HL}^1$ ,  $\text{H}_2\text{L}^2$ , and  $\text{HL}^3$  within their putative binding site in the active site of PA-Nter. (A–C): Hypothetical disposition of the best energy docking poses. The full PA-Nter protein is represented by cartoon and top-ranked energy poses as cyan ( $\text{HL}^1$ ), yellow ( $\text{H}_2\text{L}^2$ ), and magenta ( $\text{HL}^3$ ) sticks. The two metal ions are orange.

with the most favorable binding energies, the fluorobenzyl moiety of  $\text{H}_2\text{L}^2$  directs toward Arg84, similarly to L-742 001, where its benzyl ring is positioned in a narrow hydrophobic cavity comprising Arg84, Trp88, Phe105, and Leu106 (Figure 9). Interestingly, the chelating motif of  $\text{H}_2\text{L}^2$  strictly overlaps

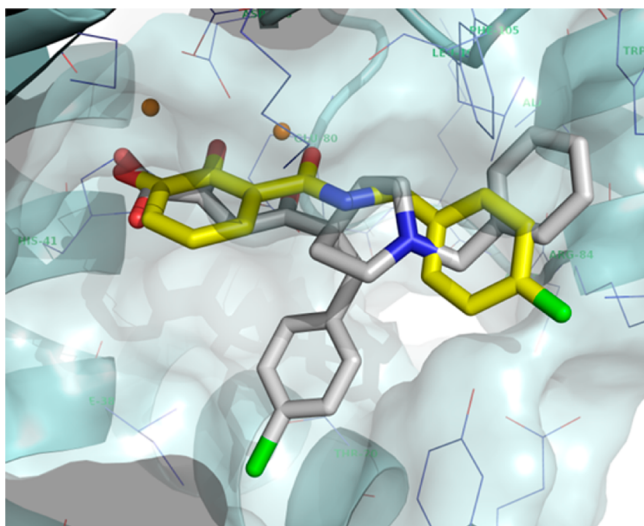


**Figure 9.** Binding model of  $\text{H}_2\text{L}^2$  (yellow) compared with the disposition of L-742 001 (gray) into the L-742 001-PA-Nter complex (PDB entry 4E5H).<sup>30</sup> The two metal ions are orange.

with the three coplanar oxygen atoms of L-742 001 (i.e., a carboxylate oxygen, a lone oxygen pair of the  $\alpha$ -hydroxyl group, and the oxygen atom at the  $\gamma$ -position), which are involved in metal chelation of the divalent ions.

Finally,  $\text{HL}^3$  behaves similarly to  $\text{HL}^1$ , since its bulky planar conformation does not result in any significant contacts with amino acid residues in the active site pocket (Figure 8C). This confirms that the PA-Nter active site is quite large and relatively shallow and therefore able to accommodate large variations in ligand size and shape with different binding affinities. Moreover, the two rotatable *p*-fluorobenzyl amides substituents at the *ortho*-position on the hydroxyl phenol group do not readily engage in a correct bridging mode for metal ion coordination and this may have a negative effect on the activity of this compound.

On the basis of these results, the inhibitory effect of  $\text{H}_2\text{L}^2$  can be explained by its arrangement in the active site of PA-Nter. In particular, the “two-metal” coordination of the cations by a unique “O,O,O” chelating triad, which is formed by an optimal combination of the catecholic and the carbonyl oxygens, appears as the important determinant for the inhibitory activity toward PA-Nter. This chelating motif therefore represents a relevant scaffold for designing novel inhibitors of the influenza virus PA endonuclease.

## CONCLUSIONS

This study was focused on the design, synthesis, and biological evaluation of a chemical scaffold containing a chelating motif able to bind one or two metal ions in the PA-Nter active site. Analysis of the potentiometric and X-ray data demonstrated the metal-complexing ability of 2-hydroxyamide-based scaffolds. All three ligands ( $\text{HL}^1$ ,  $\text{H}_2\text{L}^2$ , and  $\text{HL}^3$ ) are found to chelate  $\text{Mg}^{2+}$  ions, forming complexes with different stoichiometric ratios. However, their coordination ability was found to be different. In particular, at physiological pH, potentiometric studies proved that  $\text{H}_2\text{L}^2$  is the most efficient one, and this also resulted in inhibition of the PA-Nter endonuclease activity. Two compounds,  $\text{H}_2\text{L}^2$  and the corresponding magnesium complex **8**, proved to be effective inhibitors of the PA-Nter endonuclease activity, and it is interesting to note that complex

**8** displayed a 2-fold higher potency than its free ligand  $\text{H}_2\text{L}^2$ . As far as we know, it is the first time that an inhibition of the PA-Nter endonuclease activity by a metal complex has been reported. The results of the potentiometric studies and the molecular modeling analysis suggest that  $\text{H}_2\text{L}^2$  could interact effectively with the two metal ions in the active site of the enzyme, by using the catechol and the amide oxygen, and, in this way, it could exercise its biological activity. Regarding the activity of **8**, it is not clear whether this compound acts in the form of the starting complex, since it may rearrange under the conditions of the enzymatic assay. However, since the enzyme assay is performed with 1 mM  $\text{MnCl}_2$ , we find it unlikely that the ligand  $\text{H}_2\text{L}^2$  would be uncomplexed.

On the basis of the present data, we propose that the 2,3-dihydroxyamide chemotype represents a versatile platform for designing influenza PA endonuclease inhibitors, and studies are underway to explore this scaffold further using extensive chemical modifications.

## AUTHOR INFORMATION

### Corresponding Author

\*Tel.: +39 0521 905427.

### Author Contributions

The manuscript was written through contributions of all authors. All authors have given approval to the final version of the manuscript.

### Notes

The authors declare no competing financial interest.

## ACKNOWLEDGMENTS

“Centro Interdipartimentale Misure Giuseppe Casnati” and “Laboratorio di Strutturistica Mario Nardelli” of the University of Parma are thanked for facilities. The authors thank Dr. Andrea Brancale and Dr. Nicolino Pala for their assistance on the elaboration of the molecular modeling calculation. M.S. is grateful to “Fondazione Banco di Sardegna” for its partial financial support. A.S. is holder of a PhD grant from the Agency for Innovation by Science and Technology (IWT). This study was supported by a grant from the Geconcerteerde Onderzoeksacties (GOA/10/014) from the KU Leuven.

## REFERENCES

- (1) Reid, A. H.; Taubenberger, J. K.; Fanning, T. G. The 1918 Spanish influenza: integrating history and biology. *Microbes Infect.* **2001**, *3*, 81–87.
- (2) Smith, G. J. D.; Vijaykrishna, D.; Bahl, J.; Lycett, S. J.; Worobey, M.; Pybus, O. G.; Ma, S. K.; Cheung, C. L.; Raghwani, J.; Bhatt, S.; Peiris, J. S. M.; Guan, Y.; Rambaut, A. Origins and evolutionary genomics of the 2009 swine-origin H1N1 influenza A epidemic. *Nature* **2009**, *459*, 1122–1125.
- (3) Chowell, G.; Bertozzi, S. M.; Colchero, M. A.; Lopez-Gatell, H.; Alpuche-Aranda, C.; Hernandez, M.; Miller, M. A severe respiratory disease concurrent with the circulation of H1N1 influenza. *N. Engl. J. Med.* **2009**, *361*, 674–679.
- (4) Garten, R. J.; Davis, C. T.; Russell, C. A.; Shu, B.; Lindstrom, S.; Balish, A.; Sessions, W. M.; Xu, X.; Skepner, E.; Deyde, V.; Okomo-Adhiambo, M.; Gubareva, L.; Barnes, J.; Smith, C. B.; Emery, S. L.; Hillman, M. J.; Rivailleur, P.; Smagala, J.; De Graaf, M.; Burke, D. F.; Fouchier, R. A. M.; Pappas, C.; Alpuche-Aranda, C. M.; López-Gatell, H.; Olivera, H.; López, I.; Myers, C. A.; Faix, D.; Blair, P. J.; Yu, C.; Keene, K. M.; Dotson, P. D.; Boxrud, D.; Sambol, A. R.; Abid, S. H.; St George, K.; Bannerman, T.; Moore, A. L.; Stringer, D. J.; Blevins, P.; Demmler-Harrison, G. J.; Ginsberg, M.; Kriner, P.; Waterman, S.; Smole, S.; Guevara, H. F.; Belongia, E. A.; Clark, P. A.; Beatrice, S. T.;

- Donis, R.; Katz, J.; Finelli, L.; Bridges, C. B.; Shaw, M.; Jernigan, D. B.; Uyeki, T. M.; Smith, D. J.; Klimov, A. I.; Cox, N. J. Antigenic and genetic characteristics of swine-origin 2009 A(H1N1) influenza viruses circulating in humans. *Science* **2009**, *325*, 197–201.
- (5) Gao, R.; Cao, B.; Hu, Y.; Feng, Z.; Wang, D.; Hu, W.; Chen, J.; Jie, Z.; Qiu, H.; Xu, K.; Xu, X.; Lu, H.; Zhu, W.; Gao, Z.; Xiang, N.; Shen, Y.; He, Z.; Gu, Y.; Zhang, Z.; Yang, Y.; Zhao, X.; Zhou, L.; Li, X.; Zou, S.; Zhang, Y.; Li, X.; Yang, L.; Guo, J.; Dong, J.; Li, Q.; Dong, L.; Zhu, Y.; Bai, T.; Wang, S.; Hao, P.; Yang, W.; Zhang, Y.; Han, J.; Yu, H.; Li, D.; Gao, G. F.; Wu, G.; Wang, Y.; Yuan, Z.; Shu, Y. Human infection with a novel avian-origin influenza A (H7N9) virus. *N. Engl. J. Med.* **2013**, *368*, 1888–1897.
- (6) Krug, R. M.; Aramini, J. M. Emerging antiviral targets for influenza A virus. *Trends Pharmacol. Sci.* **2009**, *30*, 269–277.
- (7) Du, J.; Cross, T. A.; Zhou, H.-X. Recent progress in structure-based anti-influenza drug design. *Drug Discovery Today* **2012**, *17*, 1111–1120.
- (8) Reece, P. A. Neuraminidase inhibitor resistance in influenza viruses. *J. Med. Virol.* **2007**, *1586*, 1577–1586.
- (9) Collins, P. J.; Haire, L. F.; Lin, Y. P.; Liu, J.; Russell, R. J.; Walker, P. A.; Skehel, J. J.; Martin, S. R.; Hay, A. J.; Gamblin, S. J. Crystal structures of oseltamivir-resistant influenza virus neuraminidase mutants. *Nature* **2008**, *453*, 1258–1261.
- (10) Honda, A.; Ishihama, A. *Biol. Chem.* **1997**, *378*, 483–488.
- (11) Honda, A.; Mizumoto, K.; Ishihama, A. Minimum molecular architectures for transcription. *Proc. Natl. Acad. Sci. U.S.A.* **2002**, *99*, 1–6.
- (12) Plotch, S. J.; Bouloy, M.; Ulmanen, I.; Krug, R. M. *Cell* **1981**, *23*, 847–858.
- (13) Dias, A.; Bouvier, D.; Crépin, T.; McCarthy, A.; Hart, D. J.; Baudin, F.; Cusack, S.; Ruigrok, R. W. H. The cap-snatching endonuclease of influenza virus polymerase resides in the PA subunit. *Nature* **2009**, *458*, 914–918.
- (14) Yuan, P.; Bartlam, M.; Lou, Z.; Chen, S.; Zhou, J.; He, X.; Lv, Z.; Ge, R.; Li, X.; Deng, T.; Fodor, E.; Rao, Z.; Liu, Y. Crystal structure of an avian influenza polymerase PA N reveals an endonuclease active site. *Nature* **2009**, *458*, 909–913.
- (15) Crépin, T.; Dias, A.; Palencia, A.; Swale, C.; Cusack, S.; Ruigrok, R. W. H. Mutational and metal binding analysis of the endonuclease domain of the influenza virus polymerase PA subunit. *J. Virol.* **2010**, *84*, 9096–9104.
- (16) Steitz, T.; Steitz, J. A general two-metal-ion mechanism for catalytic RNA. *Proc. Natl. Acad. Sci. U.S.A.* **1993**, *90*, 6498–6502.
- (17) Doan, L.; Handa, B.; Roberts, N.; Klumpp, K. Metal ion catalysis of RNA cleavage by the influenza virus endonuclease. *Biochemistry* **1999**, *38*, 5612–9.
- (18) Rogolino, D.; Carcelli, M.; Sechi, M.; Neamati, N. Viral enzymes containing magnesium: metal binding as a successful strategy in drug design. *Coord. Chem. Rev.* **2012**, *256*, 3063–3086.
- (19) Kirschberg, T.; Parrish, J. Metal chelators as antiviral agents. *Curr. Opin. Drug Discovery Dev.* **2007**, *10*, 460–472.
- (20) Liao, C.; Marchand, C.; Burke, T. R., Jr; Pommier, Y.; Nicklaus, M. C. NIH Public Access. *Future Med. Chem.* **2010**, *2*, 1107–1122.
- (21) Tomassini, J.; Selnick, H.; Davies, M. E.; Armstrong, M. E.; Baldwin, J.; Bourgeois, M.; Hastings, J.; Hazuda, D.; Lewis, J.; McClements, W.; Ponticello, G.; Radzilowski, E.; Smith, G.; Tebben, A.; Wolfe, A. Inhibition of cap (m7GpppXm)-dependent endonuclease of influenza virus by 4-substituted 2,4-dioxobutanoic acid compounds. *Antimicrob. Agents Chemother.* **1994**, *38*, 2827–2837.
- (22) Hastings, J. C.; Selnick, H.; Wolanski, B.; Tomassini, J. E. Anti-influenza virus activities of 4-substituted 2,4-dioxobutanoic acid inhibitors. *Antimicrob. Agents Chemother.* **1996**, *40*, 1304–1307.
- (23) Tomassini, J. E.; Davies, M. E.; Hastings, J. C.; Lingham, R.; Mojena, M.; Raghoobar, S. L.; Singh, S. B.; Tkacz, J. S.; Goetz, M. A novel antiviral agent which inhibits the endonuclease of influenza viruses. *Antimicrob. Agents Chemother.* **1996**, *40*, 1189–1193.
- (24) Hensens, O. D.; Goetz, M. A.; Liesch, J. M.; Zink, D. L.; Raghoobar, S. L.; Helms, G. L.; Singh, S. B. Isolation and structure of Flutimide, a novel endonuclease inhibitor of influenza virus. *Tetrahedron Lett.* **1995**, *36*, 2005–2008.
- (25) Cianci, C.; Chung, T. D. Y.; Meanwell, N.; Putz, H.; Hagen, M.; Colonna, R. J.; Krystal, M. Identification of N-hydroxamic acid and N-hydroxymide compounds that inhibit the influenza virus polymerase. *Antiviral Chem. Chemother.* **1996**, *7*, 353–360.
- (26) Parkes, K. E.; Ermert, P.; Fässler, J.; Ives, J.; Martin, J. A.; Merrett, J. H.; Obrecht, D.; Williams, G.; Klumpp, K. Use of a pharmacophore model to discover a new class of influenza endonuclease inhibitors. *J. Med. Chem.* **2003**, *46*, 1153–1164.
- (27) Iwai, Y.; Murakami, K.; Gomi, Y.; Hashimoto, T.; Asakawa, Y. Anti-influenza activity of marchantins, macrocyclic bisbibenzyls contained in liverworts. *PLoS One* **2011**, *6*, e19825.
- (28) Kuzuhara, T.; Iwai, Y.; Takahashi, H.; Hatakeyama, D.; Echigo, N.; Bunri, T. Green tea catechins inhibit the endonuclease activity of influenza A virus RNA polymerase. *PLoS One Currents* **2012**, *1*–8.
- (29) Song, J.-M.; Lee, K.-H.; Seong, B.-L. Antiviral effect of catechins in green tea on influenza virus. *Antiviral Res.* **2005**, *68*, 66–74.
- (30) Agrawal, A.; DeSoto, J.; Fullagar, J. L.; Maddali, K.; Rostami, S.; Richman, D. D.; Pommier, Y.; Cohen, S. M. Probing chelation motifs in HIV integrase inhibitors. *Proc. Natl. Acad. Sci. U.S.A.* **2012**, *109*, 2251–2256.
- (31) Dubois, R. M.; Slavish, P. J.; Baughman, B. M.; Yun, M.; Bao, J.; Webby, R. J.; Webb, T. R.; White, S. W. Structural and biochemical basis for development of influenza virus inhibitors targeting the PA endonuclease. *PLoS Pathogens* **2012**, *8* (8), e1002830.
- (32) Kowalski, E.; Zubietta, C.; Wolkerstorfer, A.; Szolar, O. H. J.; Ruigrok, R. W. H.; Cusack, S. Structural analysis of specific metal chelating inhibitor binding to the endonuclease domain of influenza pH1N1 (2009) Polymerase. *PLoS Pathogens* **2012**, *8* (8), e1002831.
- (33) Fan, X.; Zhang, F.-H.; Al-Safi, R. I.; Zeng, L.-F.; Shabaik, Y.; Debnath, B.; Sanchez, T. W.; Odde, S.; Neamati, N.; Long, Y.-Q. Design of HIV-1 integrase inhibitors targeting the catalytic domain as well as its interaction with LEDGF/p75: a scaffold hopping approach using salicylate and catechol groups. *Biorg. Med. Chem.* **2011**, *19*, 4935–4952.
- (34) SAINT: SAX, Area Detector Integration. Siemens Analytical instruments, Inc.: Madison, WI.
- (35) SADABS: Area-Detector Absorption Correction. Siemens Industrial Automation, Inc.: Madison, WI, 1996.
- (36) Burla, M. C.; Cagliandro, R.; Camalli, M.; Carrozzini, B.; Cascarano, G. L.; De Caro, L.; Giacovazzo, C.; Polidori, G.; Spagna, R. SIR2004: an improved tool for crystal structure determination and refinement. *J. Appl. Crystallogr.* **2005**, *38*, 381–388.
- (37) SHELXL97; Sheldrick, G. M. *Acta Crystallogr.* **2008**, *A64*, 112.
- (38) Allen, F. H. The Cambridge Structural Database: a quarter of a million crystal structures and rising. *Acta Crystallogr.* **2002**, *B58*, 380–388.
- (39) Dolomanov, O. V.; Bourhis, L. J.; Gildea, R. J.; Howard, J. A. K.; Puschmann, H. OLEX2: a complete structure solution, refinement and analysis program. *J. Appl. Crystallogr.* **2009**, *42*, 339–341.
- (40) Fisicaro, E.; Braibanti, A. *Talanta* **1988**, *10*, 769.
- (41) Gran, G. *Analyst* **1952**, *77*, 661.
- (42) Gans, P.; Sabatini, A.; Vacca, A. *Talanta* **1996**, *43*, 1739.
- (43) Molecular Operating Environment (MOE 2010.11). Chemical Computing Group, Inc.: Montreal, Quebec, Canada.
- (44) Feher, M.; Williams, C. I. *J. Chem. Infect. Model* **2009**, *49*, 1704.
- (45) Zhang, Q. X.; Zhang, B. *Acta Crystallogr.* **2008**, *E 64*, o884.
- (46) Sechi, M.; Bacchi, A.; Carcelli, M.; Compari, C.; Duce, E.; Fisicaro, E.; Rogolino, D.; Gates, P.; Derudas, M.; Al-Mawsawi, L. Q.; Neamati, N. From ligand to complexes: Inhibition of human immunodeficiency virus type 1 integrase by  $\beta$ -diketo acid metal complexes. *J. Med. Chem.* **2006**, *49*, 4248–4260.
- (47) Cowan, J. Metal activation of enzymes in nucleic acid biochemistry. *Chem. Rev.* **1998**, *98*, 1067–1088.
- (48) Dudev, T.; Cowan, J.; Lim, C. Competitive binding in magnesium coordination chemistry: water versus ligands of biological interest. *J. Am. Chem. Soc.* **1999**, *121*, 7665–7673.

- (49) Cowan, J. Structural and catalytic chemistry of magnesium-dependent enzymes. *Biometals: an international journal on the role of metal ions in biology, biochemistry, and medicine* **2002**, *15*, 225–235.
- (50) Noble, E.; Cox, A.; Deval, J.; Kim, B. Endonuclease substrate selectivity characterized with full-length PA of influenza A virus polymerase. *Virology* **2012**, *433*, 27–34.